Supporting Information
Quantum effects in CH activation with $[Cu_2O_2]^{2+}$ complexes

Selin Bac,[a] Shaama Mallikarjun Sharada*[a,b]

1 Spin Correction Procedure

Removing the spin contamination of the $[Cu_2O_2]^{2+}$ core is important in identifying true energy barriers and, therefore, rate coefficients. To this end, we compute high-spin (HS) and broken-symmetry (BS) solutions (using wavefunction stability analysis) along the reaction coordinate. We perform the procedure outlined by Yamaguchi et al. to calculate spin-corrected energies.[1] The resultant barriers are shown in Table S1. The incorporation of spin-correction lowers barriers; however, the trends across systems remain largely unaltered. We elect to use unstable energies in our analysis of kinetics because fluctuations in HS energies manifest prominently in some systems, as shown in Figure S1. This choice allows us to examine the influences exerted by ligands and chain lengths alone.

2 Energy Decomposition Analysis

Energy Decomposition Analysis (EDA) can dissect the total energy of a molecular system into contributions from different intermolecular interactions. Employing the second-generation absolutely localized molecular orbital (ALMO) variant of EDA, we parse the interaction energy (E_{INT}) into various components:[2–5]

$$E_{INT} = E_{PRP} + E_{FRZ} + E_{POL} + E_{CT} \tag{1}$$

where frozen interactions (E_{FRZ}) comprise permanent electrostatics (E_{ELEC}), Pauli repulsion (E_{PAULI}), and dispersion (E_{DISP}) energies. Polarization (E_{POL}) accounts for the energy reduction due to orbital relaxation in the presence of the other fragment, while the charge transfer term (E_{CT}) arises from further interfragment orbital relaxation. We examine EDA components of the initial states for varying substrate chain lengths by partitioning them into catalyst-substrate fragments.

3 CH Activation with Dioxo-Dicopper Complexes

We investigate the effects of changing the ligand of the bis(μ-oxo) dicopper core catalyst and increasing the substrate chain length on the rate coefficients employing the variational transition state theory with multidimensional tunneling (VTST/MT). Effects of including tunneling contributions are shown in Figure S2, whereas the differences

[a] Mork Family Department of Chemical Engineering and Materials Science,
[b] Department of Chemistry, University of Southern California, Los Angeles CA 90089, USA.
E-mail: ssharada@usc.edu

Table S1: Unstable, broken-symmetry (BS), high-spin (HS), and spin-corrected (SC) energies barriers ($\Delta E^{\ddagger}$) for **Oxo** and **Rad** mechanisms across all ligand substitutions and C1-C3 substrates examined in this work. $\Delta E^{\ddagger}$ is calculated between the transition state (s=0) and the initial state. Spin-corrected energies are calculated using the scheme by Yamaguchi and coworkers.[1] All values are given in kJ mol^{-1}.

		H/C_3H_8	**H/C_2H_6**	**H/CH_4**	**OCH_3/CH_4**	**CH_3/CH_4**	**CF_3/CH_4**	**NO_2/CH_4**
Rad	Unstable	162.2	166.8	181.8	181.3	178.4	171.6	175.4
	BS	107.0	113.3	145.3	158.9	141.4	130.5	110.4
	HS	95.1	101.5	133.2	189.8	128.3	145.1	127.4
	SC	121.6	127.9	160.0	135.6	157.4	114.0	90.9
Oxo	Unstable	65.2	67.7	106.2	110.4	111.5	87.2	74.5
	BS	1.8	3.9	48.6	51.3	48.4	26.6	8.8
	HS	22.3	42.3	71.3	74.7	91.0	58.8	44.9
	SC	-20.6	-34.3	25.2	25.6	10.9	-2.0	-26.7

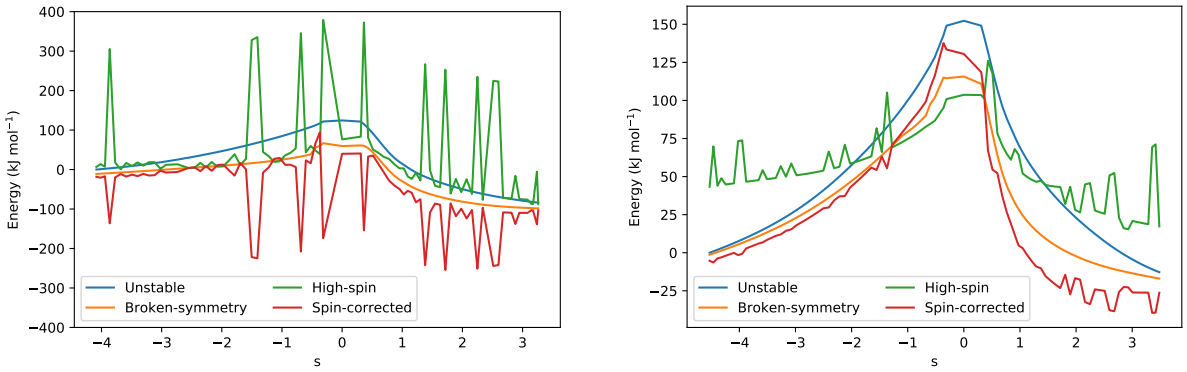

(a) **Rad** - H/CH_4 (b) **Rad** - NO_2/CH_4

Figure S1: Energy profiles obtained with spin-unstable, broken-symmetry, high-spin, and spin-corrected solutions for the radical recombination mechanism of the (a) H-substituted and (b) NO_2-substituted catalyst, and CH_4 substrate along the reaction pathway.

Table S2: Energy decomposition analysis of the reactant state for the varying chain length of the substrate. All energies are given in kJ mol^{-1}.

	$\mathbf{H/CH_4}$	$\mathbf{H/C_2H_6}$	$\mathbf{H/C_3H_8}$	$\mathbf{H/C_4H_{10}}$	$\mathbf{H/C_5H_{12}}$
$\mathbf{E_{POL}}$	-1.18	-3.87	-8.34	-6.64	-11.40
$\mathbf{E_{CT}}$	-3.86	-4.53	-7.23	-6.95	-11.68
$\mathbf{E_{ELEC}}$	-21.11	-36.22	-44.31	-49.62	-72.87
$\mathbf{E_{PAULI}}$	32.41	55.82	73.95	78.41	118.47
$\mathbf{E_{DISP}}$	-19.13	-34.17	-43.48	-49.49	-70.58
$\mathbf{E_{FRZ}}$	-7.83	-14.57	-13.85	-20.71	-24.98
$\mathbf{E_{INT}}$	-12.87	-22.97	-29.42	-34.29	-48.05

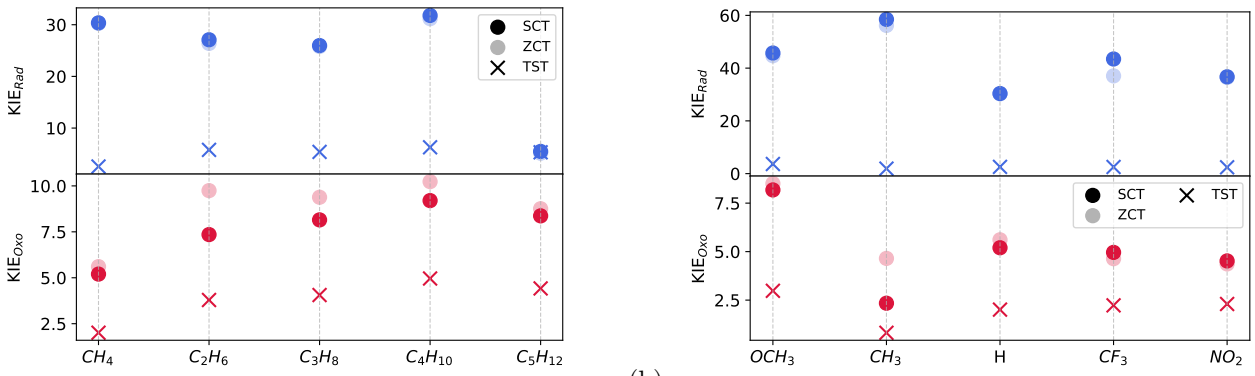

(a) (b)

Figure S2: Kinetic isotope effects at 200 K varying chain length of the substrate (a) and different ligands (b) for the two mechanisms, with and without considering tunneling effects (κ_{SCT}, κ_{ZCT} or none).

between the two tunneling coefficients, zero-curvature and small-curvature tunneling, represented by κ_{ZCT} and κ_{SCT}, respectively are shown in Figure S3.

Figure S4 shows the minimum energy paths (V_{MEP}) across substrate chain length as identified by the intrinsic reaction coordinate (IRC) calculations. Hammett plots for one-step oxo-insertion (**Oxo**) and two-step radical recombination (**Rad**) pathways are shown in Figures S5 and S6, respectively.

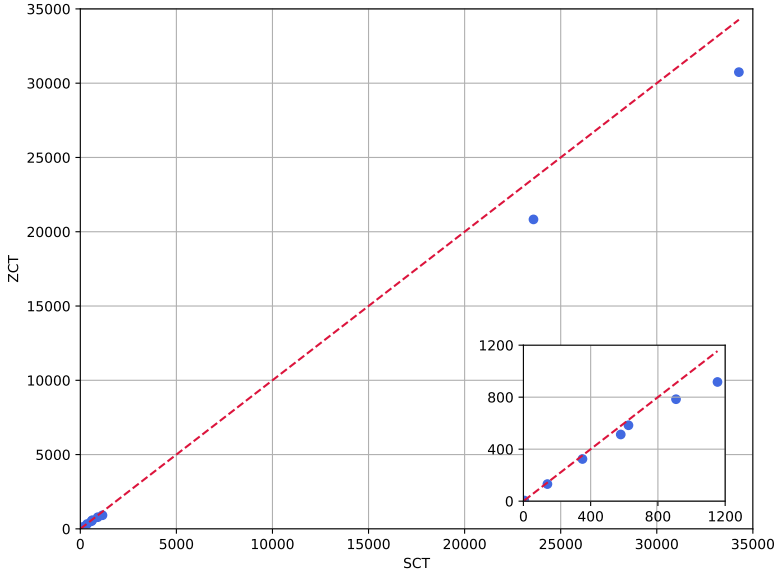

Figure S3: Comparison of small-curvature tunneling (SCT) and zero-curvature tunneling (ZCT) coefficients at 200 K represented in a parity plot. The main plot displays the full range of data, while the inset plot zooms in on lower values for ease of visualization.

The Q-Chem output files of IRC calculations are also included in Supporting Information.

(a) **Rad** - H/CH_4 (b) **Rad** - H/C_3H_8 (c) **Rad** - H/C_5H_{12}

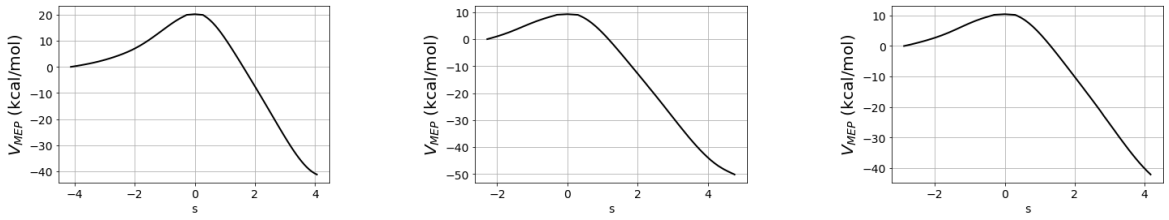

(d) **Oxo** - H/CH_4 (e) **Oxo** - H/C_3H_8 (f) **Oxo** - H/C_5H_{12}

Figure S4: Singlet potential energy profiles for two-step radical recombination and single-step oxo-insertion pathways across different substrate chain lengths.

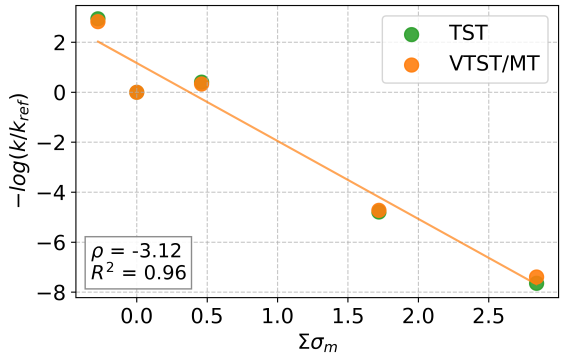

Figure S5: Hammett plot for the oxo-insertion pathway (200 K) with substituents using Hammett parameter for meta-substituted benzoic acid. The summation accounts for all four substitutions made in each catalyst. The reference rate coefficient (k_{ref}) is for the H-substituted catalyst. The R^2 value and slopes (ρ) of the linear fit are reported for VTST/MT. Without the tunneling contributions (TST), $\rho = -3.22$ and $R^2 = 0.96$.

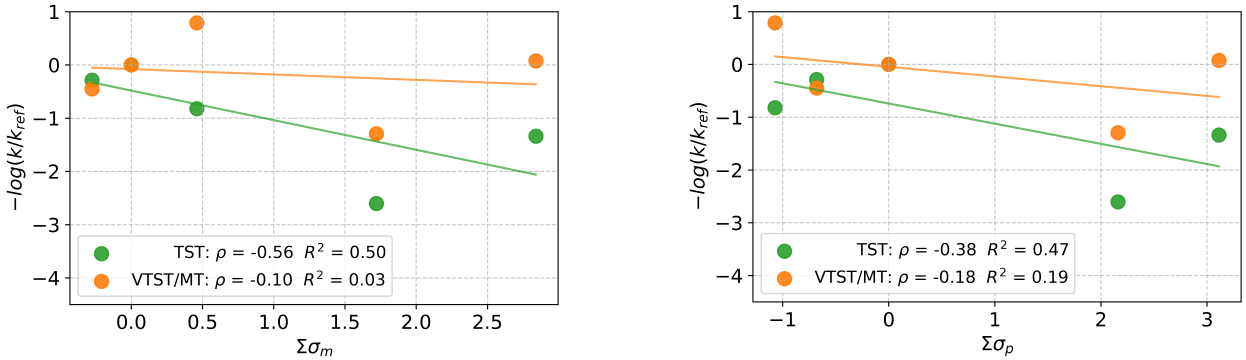

Figure S6: Hammett plots for the two-step radical recombination pathway with substituents using the Hammett parameter for meta-substituted benzoic acid (left) and para-substituted benzoic acid (right). The reference rate coefficient is for the H-substituted imidazole-bound catalyst at 200 K.

References

[1] Yamaguchi, K.; Jensen, F.; Dorigo, A.; Houk, K. A spin correction procedure for unrestricted Hartree-Fock and Møller-Plesset wavefunctions for singlet diradicals and polyradicals. *Chemical physics letters* **1988**, *149*, 537–542.

[2] Morokuma, K. Molecular orbital studies of hydrogen bonds. III. C= O··· H–O hydrogen bond in H2CO··· H2O and H2CO··· 2H2O. *The Journal of Chemical Physics* **1971**, *55*, 1236–1244.

[3] Ziegler, T.; Rauk, A. On the calculation of bonding energies by the Hartree Fock Slater method: I. The transition state method. *Theoretica Chimica Acta* **1977**, *46*, 1–10.

[4] Hopffgarten, M. v.; Frenking, G. Energy decomposition analysis. *Wiley Interdisciplinary Reviews: Computational Molecular Science* **2012**, *2*, 43–62.

[5] Zhao, L.; von Hopffgarten, M.; Andrada, D. M.; Frenking, G. Energy decomposition analysis. *Wiley Interdisciplinary Reviews: Computational Molecular Science* **2018**, *8*, e1345.